ACS APPLIED MATERIALS & INTERFACES

www.acsami.org Research Article

Superprotonic Conductivity of a Functionalized Metal–Organic Framework at Ambient Conditions

Xiao-Min Li,[⊥] Yameng Wang,[⊥] Yongbiao Mu, Jiang Liu,* Lin Zeng,* and Ya-Qian Lan

Cite This: ACS Appl. Mater. Interfaces 2022, 14, 9264–9271 Read Online

ABSTRACT: Seeking fast proton transport pathways at ambient conditions is desirable but challenging. Here, we report a strategy to synthesize a composite material with a polyoxometalate (POM) and an ionic liquid (IL) confined in stable metal–organic framework (MOF) channels through electrostatic interaction. The obtained SO_3H-IL-PMo_{12}@MIL-101 possesses fast proton transfer, and its proton conductivity can reach 1.33×10^{-2} S cm^{-1} at ambient conditions (30 °C, 70% relative humidity (RH)), which is the highest value among the MOF-based proton conductors operated in an ambient environment. Therefore, it has the potential of becoming a room-temperature proton conductor without a humidifier. Importantly, the composite material is further fabricated into a composite membrane for proton-exchange membrane fuel cells (PEMFCs), which can deliver a power density of 0.93 mW cm^{-2} at 30 °C and 98% RH. This result can lay a fundamental basis for the application of MOF-based proton conductors in the area of electrochemical energy conversion.

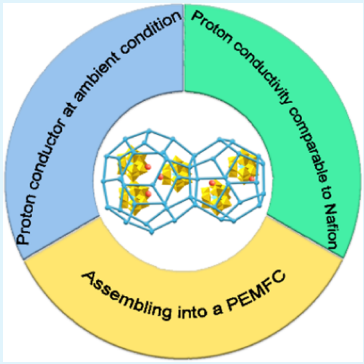

KEYWORDS: *functionalized metal–organic framework, electrostatic interaction, superprotonic conductivity, ambient condition, proton-exchange membrane fuel cell*

1. INTRODUCTION

Proton-exchange membrane fuel cells (PEMFCs) have become one of the new generations of alternative energy devices, among which a proton-exchange membrane (PEM) with high proton conductivity and mechanical stability is an essential component of PEMFCs.[1−6] Commercial perfluorinated sulfonic acids (PFSA, such as Nafion) assembled with tetrafluoroethylene hydrophobic skeletons and hydrophilic sulfonic side chains have been widely used, and their proton conductivities can reach 10^{-2} to 10^{-1} S cm^{-1} at 30−80 °C and 90−100% relative humidity (RH).[7,8] However, the high proton conductivity of PFSA depends on high humidity continuously provided by the humidifier, which requires a complex water management system and high capital cost, resulting in having a certain impact on its use in broader conditions.[9−11] Therefore, it is necessary and meaningful to seek a kind of proton-conducting material with high proton conductivity, low cost, and stable structure at ambient conditions.[12,13]

Ionic liquids (ILs) are ideal candidate materials for safe electrolytes in electrochemical devices due to their low volatility, noncombustibility, good conductivity, and high thermal stability.[14,15] Recently, metal–organic frameworks (MOFs) are considered as emerging host materials to encapsulate ILs to achieve solid-state electrolytes due to their regular and well-defined pores.[16−19] MOF channels have strong adsorption of ILs because of their high porosity and surface area, which can stabilize ILs in MOF cavities, preventing the leakage of ILs and attaining highly efficient proton transport.[20−22] On the other hand, the open channels of MOFs have a positive effect on the contact between protons and electrodes, which can also promote efficient proton transport.[23−25] Therefore, ILs can be loaded into the pores of MOFs, which can not only form effective proton transport pathways in the well-defined channels but also overcome the defect of leakage risk of ILs.[16]

To further improve proton conductivity and stability of the composite, a polyoxometalate (POM) that is a kind of anion transition-metal oxide cluster[26−28] with the characteristics of proton conduction was chosen as a guest molecule to be encapsulated into the MOF pores.[29,30] Previous studies have indicated that POM is one of the candidates for electrolyte materials in PEMFC.[31,32] Moreover, there are also some works to encapsulate POMs into the ordered channels of MOFs to achieve high proton conductivity due to supplementary proton hopping sites and increased water holding capacity.[30]

Considering the aforementioned feasibility, a new strategy of preparing a proton-conducting composite (denoted as **SO_3H-IL-PMo_{12}@MIL-101**) based on MOF, IL, and POM with high proton conductivity is proposed (Figure 1a). The well-known MIL-101 ($Cr_3(H_2O)_2O[(O_2C)C_6H_4(CO_2)]_3 \cdot nH_2O$) with a

Received: January 10, 2022
Accepted: January 28, 2022
Published: February 9, 2022

https://doi.org/10.1021/acsami.2c00500
ACS Appl. Mater. Interfaces 2022, 14, 9264−9271

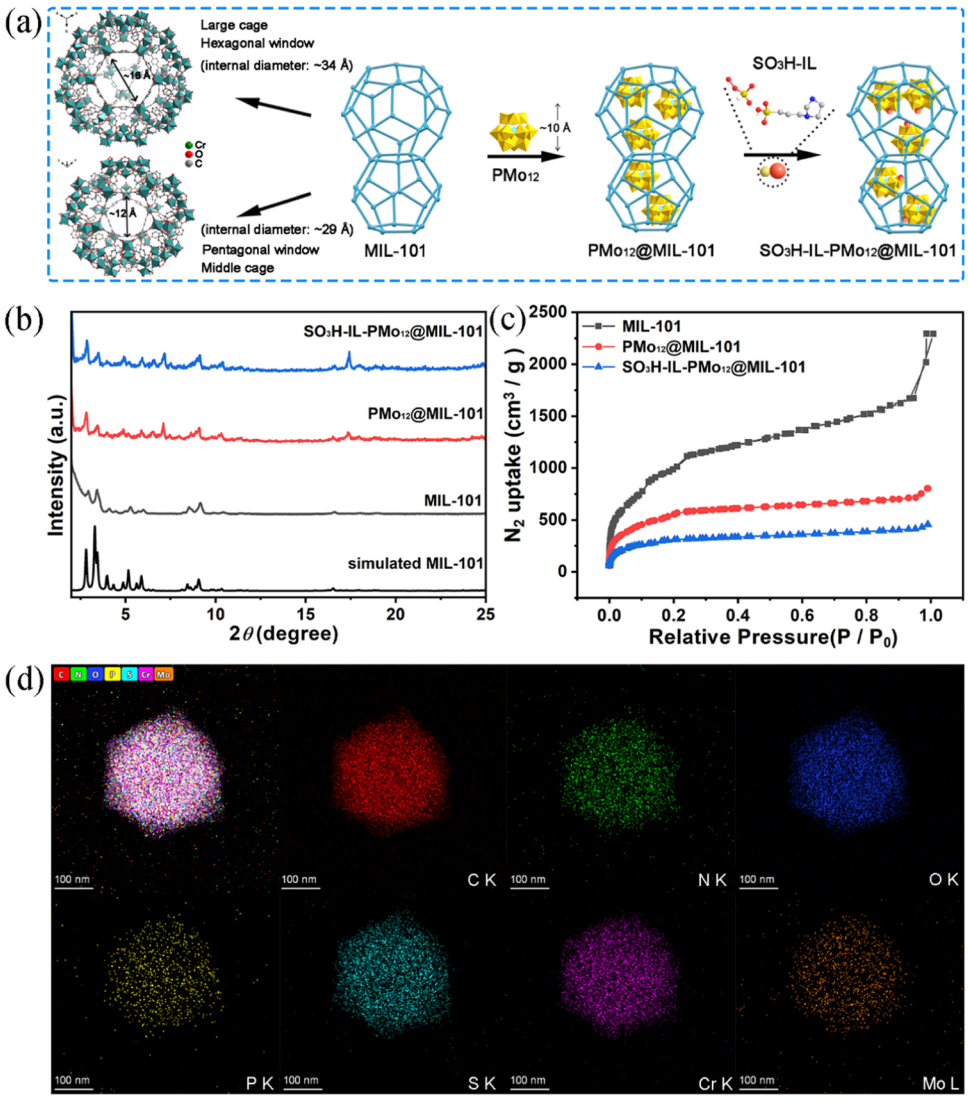

Figure 1. (a) Schematic illustration of the preparation of **SO_3H-IL-PMo_{12}@MIL-101**. (b) Powder X-ray diffraction (PXRD) patterns of simulated MIL-101 (black), as-synthesized MIL-101 (gray), as-synthesized PMo_{12}@MIL-101 (red), and as-synthesized **SO_3H-IL-PMo_{12}@MIL-101** (blue). (c) N_2 absorption−desorption isotherms of as-synthesized MIL-101 (gray), as-synthesized PMo_{12}@MIL-101 (red), and as-synthesized **SO_3H-IL-PMo_{12}@MIL-101** (blue). (d) Element mapping images of **SO_3H-IL-PMo_{12}@MIL-101** (C, N, O, P, S, Cr, and Mo).

highly stable skeleton is adopted as the host framework to provide superlarge channels for accommodating guest molecules[33] and make solid electrolytes possible. Then, PMo_{12} ($H_3PMo_{12}O_{40}{\cdot}nH_2O$) with rich oxygen atoms[34] is selected to insert into the cages of MIL-101 to get PMo_{12}@MIL-101 by a hydrothermal method, which not only increases the chemical stability and hydrophilicity but also improves proton hopping sites of the composite.[30] Eventually, the sulfonic acid-functionalized ionic liquid, SO_3H-IL ([SO_3H-$(CH_2)_3$-HIM][HSO_4]),[35] is introduced to modify PMo_{12}@MIL-101 by means of anionic exchange for encapsulating sulfonate and imidazole groups to obtain **SO_3H-IL-PMo_{12}@MIL-101**, which can further improve the proton sources and proton hopping sites. It exhibits an ultrahigh proton conductivity of 1.76×10^{-1} S cm^{-1} at 70 °C and 98% RH, which surpasses the vast majority of proton conductors and can be comparable to PFSA (Nafion).[1,36,37] It is also noteworthy that **SO_3H-IL-PMo_{12}@MIL-101** shows a high proton conductivity of 1.33×10^{-2} S cm^{-1} at ambient conditions (30 °C, 70% RH). This result not only broadens the application conditions of proton conductors but also reduces the cost of maintaining humidity, ultimately making room-temperature PEM possible.

2. RESULTS AND DISCUSSION

Microcrystalline powders of MIL-101 were fabricated by a hydrothermal method according to the previous literature. From the PXRD patterns, it can be seen that the as-synthesized MIL-101 has high purity due to its consistency with the simulated curve (Figure 1b). As for the post-modification composites, PMo_{12}@MIL-101 and **SO_3H-IL-PMo_{12}@MIL-101** also maintain the integrity of the host framework of MIL-101 because their PXRD patterns overlap with that of the parent material (Figure 1b). Moreover, measurements of N_2 adsorption−desorption isotherms of the three compounds were carried out at 77 K (Figure 1c). Compared with the large nitrogen uptake capacity of MIL-101, the dramatic descending adsorption capacities of PMo_{12}@MIL-101 and **SO_3H-IL-PMo_{12}@MIL-101** indicate that post-modification molecules have been inserted into the pores of pristine MIL-101.

https://doi.org/10.1021/acsami.2c00500
ACS Appl. Mater. Interfaces 2022, 14, 9264−9271

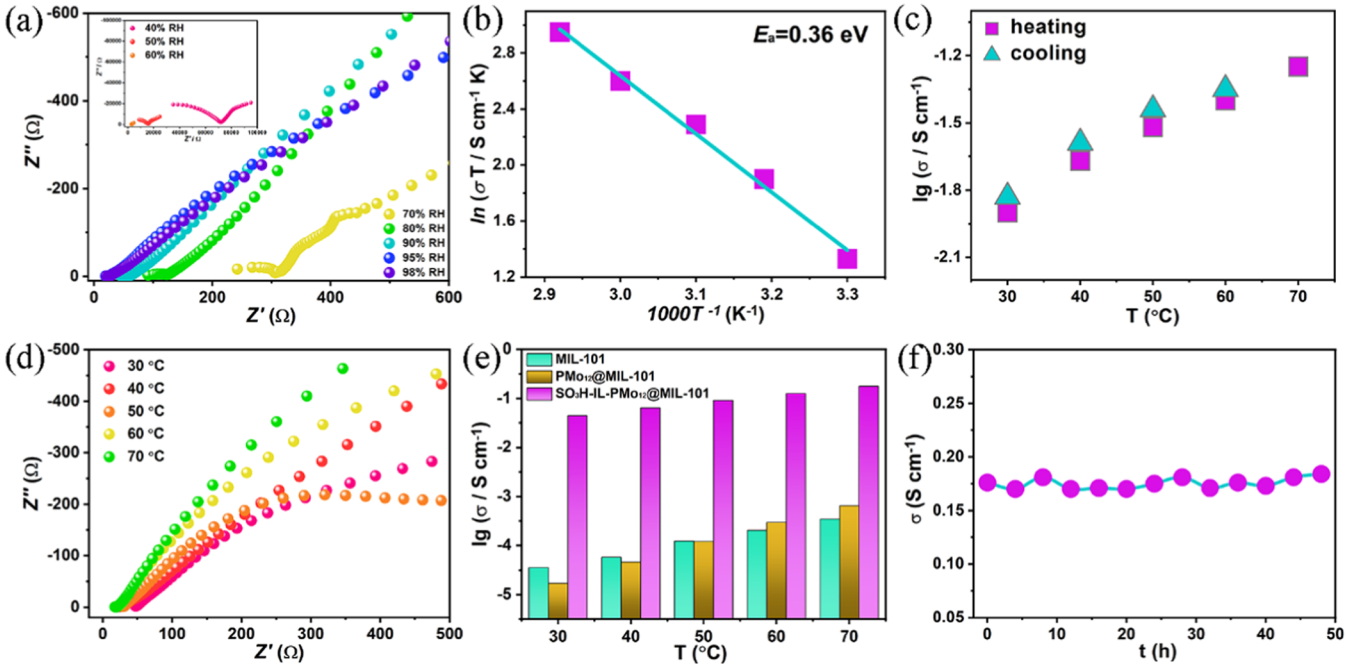

Figure 2. (a) Nyquist plots from AC impedance data of **SO_3H-IL-PMo_{12}@MIL-101** at 30 °C and different humidity variations from 40 to 98% RH. (b) Arrhenius plot of **SO_3H-IL-PMo_{12}@MIL-101** under 70% RH and in the temperature range of 30−70 °C. (c) Proton conductivities for the heating−cooling cycle of **SO_3H-IL-PMo_{12}@MIL-101** at 70% RH and within the temperature range of 30−70 °C. (d) Nyquist plots from AC impedance data of **SO_3H-IL-PMo_{12}@MIL-101** at 98% RH and different temperature variations from 30 to 70 °C. (e) Temperature-dependent proton conductivities of MIL-101 (pale blue), PMo_{12}@MIL-101 (yellow), and **SO_3H-IL-PMo_{12}@MIL-101** (rose red) (98% RH, 30−70 °C). (f) Time-dependent proton conductivities of **SO_3H-IL-PMo_{12}@MIL-101** performed at 70 °C and 98% RH.

Meanwhile, the surface morphologies of MIL-101, PMo_{12}@MIL-101, and **SO_3H-IL-PMo_{12}@MIL-101** were studied by scanning electron microscopy (SEM) and transmission electron microscopy (TEM) (Figures S1−S6). The original MIL-101 has a regular octahedral geometry structure, and its surface is relatively smooth (Figure S1). The crystal morphology of PMo_{12}@MIL-101 slightly decreases smoothly because of encapsulating PMo_{12} in cages (Figure S2). As shown in Figure S3, the surface of **SO_3H-IL-PMo_{12}@MIL-101** becomes rough owing to the grafting of a heteropolyanionic ionic liquid, but its overall morphology is still similar to MIL-101. Furthermore, as shown in Figure 1d, **SO_3H-IL-PMo_{12}@MIL-101** contains the elements that originated from the combination of MIL-101, PMo_{12}, and SO_3H-IL. The results of energy-dispersive X-ray (EDX) and inductively coupled plasma (ICP) shown in Figures S7−S9 and Tables S1, S2 further verify that there are 0.15 PMo_{12} and 0.45 SO_3H-IL encapsulated in a MIL-101 unit. In view of the above facts, it can be evidently proved that PMo_{12} and SO_3H-IL were successfully encapsulated into the channels of the host framework. Thermogravimetric analysis curves of MIL-101, PMo_{12}@MIL-101, and **SO_3H-IL-PMo_{12}@MIL-101** are shown in Figure S10, where the decreases in the first platform before 150 °C are caused by the loss of guest molecules (H_2O).[38] It can be seen that MIL-101 has the most weight loss, while PMo_{12}@MIL-101 and **SO_3H-IL-PMo_{12}@MIL-101** have reduced weight loss because the cages of MIL-101 are occupied by guest molecules.[39] In the second step (150−350 °C), the weight loss corresponding to the water molecules coordinated with chromium is observed. In the last step (350−550 °C), the weight loss is attributed to the collapse of the framework of MIL-101 originating from the decomposition of terephthalic acid. In addition, the difference of weight loss between PMo_{12}@MIL-101 and **SO_3H-IL-PMo_{12}@MIL-101** may be related to the decomposition of the sulfonic acid anion in the cavity.[39] Obviously, the introduction of PMo_{12} and SO_3H-IL increases the thermal stability of the composite and makes it have more potential applications in a wider temperature range.

On the basis of as-synthesized samples, we measured their proton conductivities at a fixed temperature of 30 °C and within the humidity range of 40−98% RH employing alternating current (AC) impedance spectroscopy (Figures S11, S12, and 2a). It can be known that the semicircle of the high frequency relates to the resistance contributions of bulk and grain boundary, and the tail of the low frequency corresponds to the resistance contribution of mobile ions in the interface between the electrode and electrolyte.[40,41] As shown in Figure S13, a positive correlation between the proton conductivity and humidity can be observed. These monotonically increasing proton conductivities show that water molecules play a role in proton conduction, which influences the effective proton transport because water molecules form proton carriers in the form of $H_2O-H_3O^+$ for proton hopping.[40] It can be seen from H_2O adsorption measurements at 298 K that the H_2O adsorption capacity of MIL-101 is the largest, which may be caused by its large pore space that can absorb a large number of H_2O molecules into the pores (Figure S14). However, the H_2O adsorption capacity of **SO_3H-IL-PMo_{12}@MIL-101** is minimum, which indicates that SO_3H-IL and PMo_{12} have occupied its channels. Although the sulfonic acid group is hydrophilic, the effect of decreased pore volume seems to become dominant. It can be analyzed that the contributions of proton sources and proton carriers from **SO_3H-PMo_{12}@MIL-101** itself to its proton conductivity are significant. Meanwhile, it should be noted that the proton conductivity of **SO_3H-IL-PMo_{12}@MIL-101** at 30 °C and 70%

https://doi.org/10.1021/acsami.2c00500
ACS Appl. Mater. Interfaces 2022, 14, 9264−9271

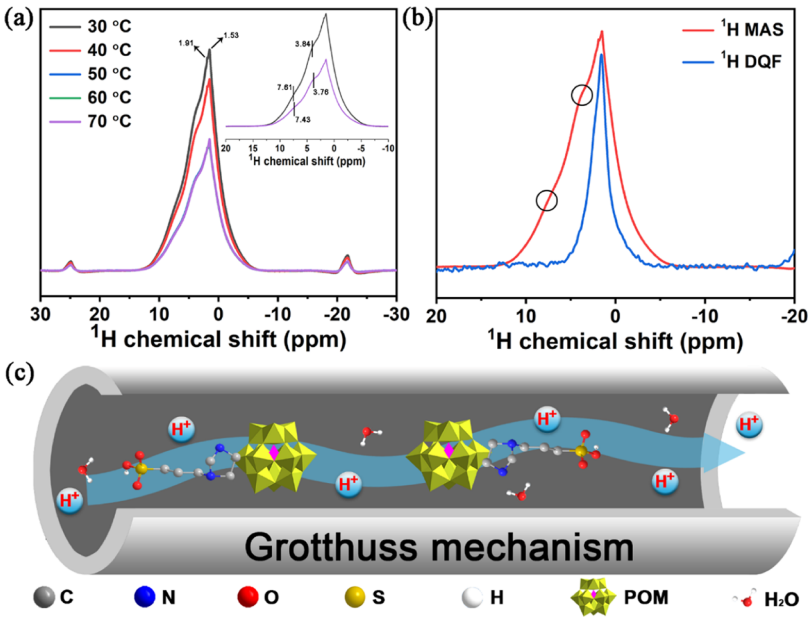

Figure 3. (a) ^{1}H VT-SSNMR spectra of **SO_3H-IL-PMo_{12}@MIL-101** at the temperature range of 30−70 °C (inset: partial enlarged SSNMR spectra at 30 and 70 °C). (b) Comparison of the ^{1}H MAS (red) SSNMR spectrum and ^{1}H DQF (blue) SSNMR spectrum of **SO_3H-IL-PMo_{12}@MIL-101** at room temperature. (c) Schematic of the proton transport pathway constructed by POMs, ILs, and water molecules arranged in the channels of MIL-101.

RH is 1.33×10^{-2} S cm^{-1} (Figure S15), which is a desired and rare value at ambient conditions (Table S3). It can be observed that there are three semicircles in the high-frequency region, which correspond to bulk, grain boundary, and electrode resistances.[42] The resistance was fitted through the higher-frequency semicircle.[41] This study provides a wider range of conditions for the practical application of proton conductors and makes it possible to apply proton conductors at ambient conditions. Additionally, the host structures of MIL-101, PMo_{12}@MIL-101, and **SO_3H-IL-PMo_{12}@MIL-101** after H_2O adsorption measurements were maintained, which was proved by the result of PXRD patterns (Figure S16).

The thermodynamics also has a certain influence on the proton movement, so the temperature dependence tests of **SO_3H-IL-PMo_{12}@MIL-101** at 70% RH were conducted (Figures S17a). The proton conductivity increases with the increasing temperature and it can reach 5.57×10^{-2} S cm^{-1} at 70 °C (70% RH) (Figure S18). According to the Arrhenius equation, the activation energies (E_a) of **SO_3H-IL-PMo_{12}@MIL-101** at 70% RH and different temperatures were calculated to determine its proton transfer mechanism. The E_a value of **SO_3H-IL-PMo_{12}@MIL-101** at 70% RH is 0.36 eV, which can be assigned to the Grotthuss mechanism, which is indicative of fast proton transport occurring in its channels (Figure 2b). Moreover, the heating−cooling cycle performance stability of **SO_3H-IL-PMo_{12}@MIL-101** at 70% RH was evaluated (Figure S17). As shown in Figure 2c, it can be observed that there is almost no change in the proton conductivity at the same temperature during the cycle, which indicates that **SO_3H-IL-PMo_{12}@MIL-101** has an excellent temperature cycle performance stability. Meanwhile, there is almost no difference for **SO_3H-IL-PMo_{12}@MIL-101** in activation energy during the cycle measurements, which illustrates the consistency of the proton transport mechanism (Figure S19).

To test the durability of the performance of **SO_3H-IL-PMo_{12}@MIL-101** at 30 °C and 70% RH, its time-dependent proton conductivities were measured. Notably, the proton conductivity of **SO_3H-IL-PMo_{12}@MIL-101** is well maintained after continuous operation for 48 h with negligible loss, which exhibits that it has the potential as an electrolyte in a fuel cell that works in the ambient environment without a humidifier (Figure S20).

Furthermore, temperature dependence tests of MIL-101, PMo_{12}@MIL-101, and **SO_3H-IL-PMo_{12}@MIL-101** were conducted (Figures S21, S22, and 2d). Figures S23−S25 depict the Nyquist plots of MIL-101, PMo_{12}@MIL-101, and **SO_3H-IL-PMo_{12}@MIL-101**, respectively, at 70 °C and 98% RH from which it can be seen that the resistance of **SO_3H-IL-PMo_{12}@MIL-101** is the lowest. The proton conductivity increases with the increasing temperature and it can be obviously seen that **SO_3H-IL-PMo_{12}@MIL-101** has a significant advantage in the proton conduction due to the synergistic effect of multiple proton sources and proton hopping sites (Figure 2e). Moreover, the imidazole group is greatly affected by temperature, and its effect on the proton conduction is positive when the temperature increases. As a result, the proton conductivity of **SO_3H-IL-PMo_{12}@MIL-101** can reach 1.76×10^{-1} S cm^{-1} at 70 °C and 98% RH, which is one of the highest values in previously reported MOF-based proton conductors (Table S4). The proton conductivity of **SO_3H-IL-PMo_{12}@MIL-101** is about three orders of magnitude higher than those of PMo_{12}@MIL-101 (6.39×10^{-4} S cm^{-1}) and MIL-101 (3.45×10^{-4} S cm^{-1}) at 70 °C and 98% RH. It can also be seen that there is no significant difference between MIL-101 and PMo_{12}@MIL-101 in the proton conductivity. The proton conductivity of PMo_{12}@MIL-101 gradually exceeds that of MIL-101, which leads to the speculation that the effect of rapid movement of PMo_{12} in response to temperature is greater than the effect of H_2O molecules in MIL-101 pores on the proton conduction.

https://doi.org/10.1021/acsami.2c00500
ACS Appl. Mater. Interfaces 2022, 14, 9264−9271

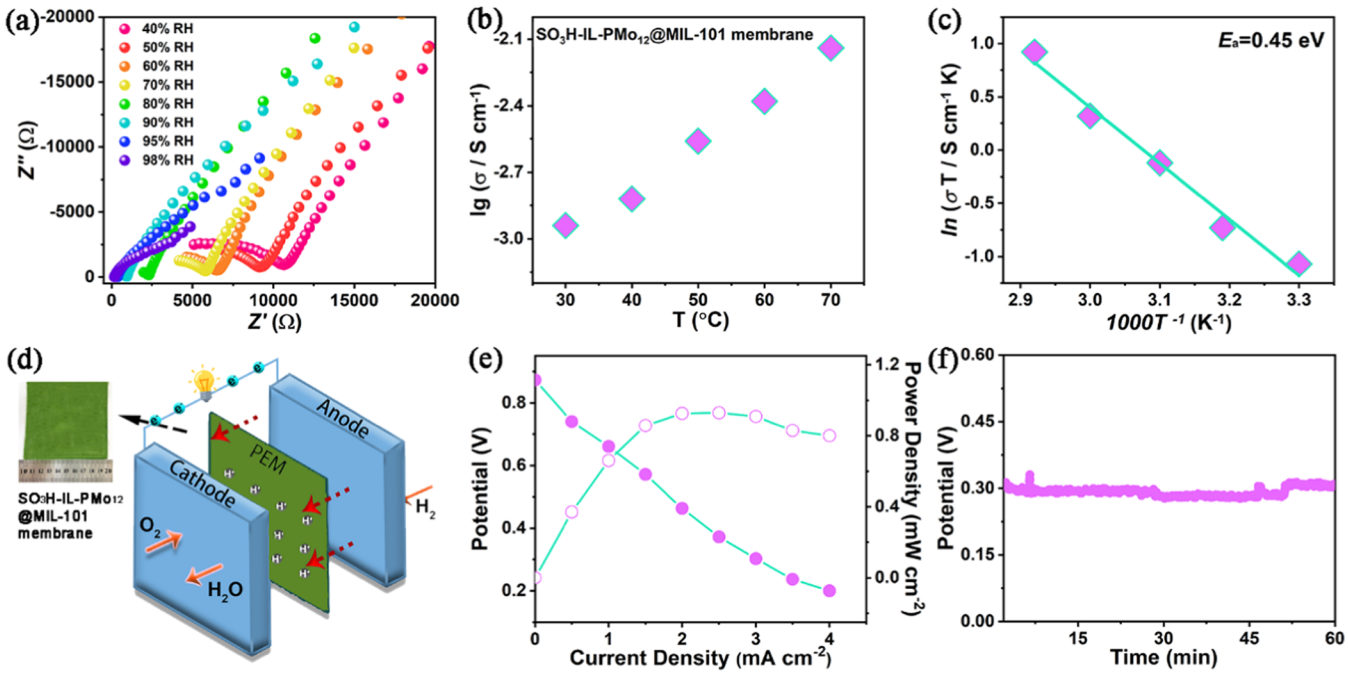

Figure 4. (a) Nyquist plots from AC impedance data of the **SO_3H-IL-PMo_{12}@MIL-101** membrane at 30 °C and different humidity variations from 40 to 98% RH. (b) Log-scaled proton conductivities of the **SO_3H-IL-PMo_{12}@MIL-101** membrane at 98% RH and different temperature variations from 30 to 70 °C. (c) Arrhenius plot of the **SO_3H-IL-PMo_{12}@MIL-101** membrane under 98% RH and in the temperature range of 30−70 °C. (d) Scheme of the PEMFC assembled with the **SO_3H-IL-PMo_{12}@MIL-101** membrane as the PEM. (e) Performance of a PEMFC with the **SO_3H-IL-PMo_{12}@MIL-101** membrane as the electrolyte at 30 °C and 98% RH. The green solid sphere and green hollow spheres represent current−voltage and current−power measurements, respectively. (f) Stability of a PEMFC with the **SO_3H-IL-PMo_{12}@MIL-101** membrane measured at 4 mA cm^{-2} at 30 °C and 98% RH.

The activation energies of MIL-101, PMo_{12}@MIL-101, and **SO_3H-IL-PMo_{12}@MIL-101** at 98% RH and within the temperature range of 30−70 °C were calculated through the Arrhenius equation to determine their proton transfer modes. It can be obviously known that the proton transfer mechanisms of MIL-101 (E_a = 0.56 eV) and PMo_{12}@MIL-101 (E_a = 0.90 eV) belong to the vehicle mechanism (Figures S26 and S27), while the proton transfer mechanism of **SO_3H-IL-PMo_{12}@MIL-101** (E_a = 0.32 eV) can be assigned to the Grotthuss mechanism (Figure S28). The reason why the E_a value of PMo_{12}@MIL-101 is higher than that of MIL-101 may be that the PMo_{12} molecule is large, which limits the proton transfer rate of PMo_{12}@MIL-101. As for **SO_3H-IL-PMo_{12}@MIL-101**, hydrophilic sulfonic groups are more likely to combine with the adjacent H_2O molecules, effectively transporting protons through multiple hopping sites, resulting in lower activation energy.

To test whether **SO_3H-IL-PMo_{12}@MIL-101** can meet the excellent heating−cooling cycle performance of the electrolyte in a fuel cell at 98% RH, its cycle performance was carried out (Figure S29). As shown in Figure S30, it can be observed that there is almost no change in the proton conductivity at the same temperature during the cycle, which indicates that the IL and PMo_{12} do not suffer escape, phase transition, and sublimation/evaporation when the temperature changes. Meanwhile, there is almost no difference of **SO_3H-IL-PMo_{12}@MIL-101** in activation energy during the cycle measurements, which illustrates the consistency of the proton transport mechanism (Figure S31). The results demonstrate that **SO_3H-IL-PMo_{12}@MIL-101** possesses good cycle performance stability.

With the aim of further testing the reliability of the ultrahigh performance of **SO_3H-IL-PMo_{12}@MIL-101**, its time-dependent proton conductivities at 70 °C and 98% RH were measured. It is worth noting that the proton conductivity of **SO_3H-IL-PMo_{12}@MIL-101** is well maintained after continuous operation for 48 h with negligible loss, which exhibits that it also has the potential as an electrolyte in a fuel cell that works in the humidity environment (Figure 2f). More importantly, the three materials all have the structural robustness seen from the PXRD patterns and FTIR spectra after undergoing proton conductivity measurements (Figures S32−S35). The differences of FTIR spectra between before and after proton conductivity measurements are the emergence of peaks located in 4000−3000 cm^{-1}, which may be due to the residual water molecules with O−H groups.

To have a deeper understanding of the proton transfer mechanism of **SO_3H-IL-PMo_{12}@MIL-101**, solid-state nuclear magnetic resonance (SSNMR) spectra were measured (Figure 3a,b). It can be seen from the ^1H SSNMR spectrum at 30 °C that there are four resonances at 7.61, 3.84, 1.91, and 1.53 ppm, which can be assigned to the characteristic signals of O−H from the sulfonic acid group (7.61 ppm), N−H from the imidazole group (3.84 ppm), and C−H from MOF and IL (1.91 and 1.53 ppm), respectively (Figure 3a).[43−46] As the temperature is increased to 70 °C, the feature peaks of O−H and N−H shift to lower frequencies, while the feature peak of C−H has no change, implying that fast proton motion has occurred in MIL-101 channels.[43] On the other hand, proton dynamics of **SO_3H-IL-PMo_{12}@MIL-101** are also studied by the comparison of ^1H magic-angle spinning (MAS) and ^1H double-quantum filter (DQF) SSNMR spectra at room temperature (Figure 3b). It can be observed that the feature

https://doi.org/10.1021/acsami.2c00500
ACS Appl. Mater. Interfaces 2022, 14, 9264−9271

peaks of O−H and N−H in the ^{1}H DQF spectrum disappear compared with those in the ^{1}H MAS spectrum, which is because of the weak dipole−dipole coupling caused by too long distances between protons or too fast proton transfer.[43,44] Nevertheless, the distances between proton pairs are not long because the MIL-101 pores are filled with proton carriers originating from guest molecules.[19] That is, fast proton transport occurs in the MIL-101 channels, which is a necessary condition for high proton conductivity. Meanwhile, the possible proton transfer pathways in the MIL-101 channels are analyzed through the MOF definite crystal structure and guest molecular structures. As depicted in Figure 3c, the multiple proton carriers from sulfonic acid groups, imidazole groups, and water molecules form orderly and efficient proton transport pathways, which is beneficial to obtain high proton conductivity. In addition, **SO_3H-IL-PMo_{12}@MIL-101** can absorb more H_2O molecules from the environment owing to the hydrophilicity of sulfonic acid groups, which can increase the concentration of proton carriers to improve proton transport efficiency. Moreover, both the contributions from MIL-101 and POM play important roles in enhancing the safety and stability of the system. MIL-101 provides large space for accommodating guest molecules. On the other hand, POM can stabilize IL in the pores of MIL-101 through the electrostatic interaction between IL and POM. Therefore, it can be concluded that **SO_3H-IL-PMo_{12}@MIL-101** is an excellent candidate for a safe and stable proton conductor.

To study the potential of **SO_3H-IL-PMo_{12}@MIL-101** in practical application, **SO_3H-IL-PMo_{12}@MIL-101** was used as a filler and poly(vinylidene difluoride) (PVDF)−poly(vinylpyrrolidone) (PVP) was used as a carrier to prepare the composite membrane (Figures S36 and S37). Figure S38 displays the morphology of the **SO_3H-IL-PMo_{12}@MIL-101** membrane. The mechanical property of the **SO_3H-IL-PMo_{12}@MIL-101** membrane is also assessed as shown in Figure S39 and Table S5, from which it can be seen that the elastic modulus and the ultimate tensile strength are 39.34 and 2.23 MPa, respectively. The following evaluation is to test its proton conductivities under the conditions of different humidities or different temperatures (Figures 4a and S40). The impacts of humidity and temperature on the proton conductivity of the **SO_3H-IL-PMo_{12}@MIL-101** membrane are exhibited in Figures S41 and 4b, from which it can be known that both humidity and temperature are positively related to the proton conductivity of the **SO_3H-IL-PMo_{12}@MIL-101** membrane. The proton conductivity of the **SO_3H-IL-PMo_{12}@MIL-101** membrane can ultimately reach 7.30×10^{-3} S cm^{-1} at 70 °C and 98% RH, which is a high value in the MOF-based PEMs that only conducts protons on the basis of the filler itself of MOF (Table S6). Temperature-dependent measurements to the proton conductivity of the **SO_3H-IL-PMo_{12}@MIL-101** membrane can also obtain its Arrhenius plot in the proton transportation, from which it can be calculated that the E_a value is 0.45 eV, representing a mixed mechanism of Grotthuss and vehicle mechanisms (0.4−0.5 eV) (Figure 4c).[47,48] The vehicle mechanism may be caused by the reduced proton concentration due to the supplementary membrane carriers (PVDF−PVP).[19] Furthermore, the XRD pattern after the proton conductivity test of the **SO_3H-IL-PMo_{12}@MIL-101** membrane is almost consistent with that of the as-synthesized one, implying its structural stability (Figure S42).

To explore the possibility of the practical application of the **SO_3H-IL-PMo_{12}@MIL-101** membrane as an electrolyte in PEMFC, a membrane−electrode assembly (MEA) was prepared (Figure 4d). The performance results are displayed in Figure 4e, from which it can be known that the maximum open-circuit voltage and maximum power density are 0.873 V and 0.93 mW cm^{-2}, respectively, at 30 °C and 98% RH. Moreover, the stability of the PEMFC with the **SO_3H-IL-PMo_{12}@MIL-101** membrane as the electrolyte was evaluated at 30 °C and 98% RH. As shown in Figure 4f, the potential has almost no degradation within 60 min, showing the assembled PEMFC has a good performance stability.

3. CONCLUSIONS

In summary, we successfully fabricated **SO_3H-IL-PMo_{12}@MIL-101** as a proton conductor by modifying MIL-101 pores with PMo_{12} and SO_3H-IL, in which PMo_{12} and SO_3H-IL were fixed in the channels by electrostatic attraction. It exhibited a proton conductivity of 1.76×10^{-1} S cm^{-1} at 70 °C and 98% RH, which was comparable to those of MOF-based proton conductors as reported in previous literature studies, showing that it has the potential to become a water-dependent proton conductor. More importantly, **SO_3H-IL-PMo_{12}@MIL-101** shows a high proton conductivity of 1.33×10^{-2} S cm^{-1} under ambient conditions of 30 °C and 70% RH, meaning that it has the potential of a proton conductor working in the ambient environment without a humidifier. Moreover, the corresponding membrane (**SO_3H-IL-PMo_{12}@MIL-101** membrane) was prepared and then assembled into a PEMFC as an electrolyte, which represents further potential suitability of the material used as a PEM.

4. EXPERIMENTAL SECTION

4.1. Synthesis of PMo_{12}@MIL-101. MIL-101 (0.2 g) and PMo_{12} (0.2 g) were dissolved in distilled water (50 mL). Subsequently, the solution was transferred into a 100 mL autoclave and heated at 140 °C for 12 h. The resulting precipitate was collected by centrifugation and washed with distilled water and ethanol. After drying at 80 °C overnight on a vacuum oven, the final material was obtained.

4.2. Synthesis of SO_3H-IL-PMo_{12}@MIL-101. Excessive IL was dissolved in ethanol (20 mL), and then PMo_{12}@MIL-101 (0.2 g) was added into the solution. Subsequently, the solution was stirred at room temperature for 48 h. Then, the mixture was washed by centrifugation with ethanol several times. After drying at 80 °C overnight on a vacuum oven, the final material was obtained.

4.3. Synthesis of the SO_3H-IL-PMo_{12}@MIL-101 Membrane. **SO_3H-IL-PMo_{12}@MIL-101** (675 mg) was sonically dispersed in *N*,*N*-dimethylformamide (DMF) (6 mL) for 1 h. Subsequently, PVDF (135 mg) and PVP (315 mg) were added into the above dispersion and then the mixture was stirred at room temperature overnight to get a homogeneous jelly, which was poured into a mold with poly(tetrafluoroethylene) (PTFE). After drying at 80 °C for 6 h, the membrane was obtained. When the temperature dropped to room temperature, the membrane was taken off the mold and then washed with distilled water. Finally, the **SO_3H-IL-PMo_{12}@MIL-101** membrane was dried in air for further measurements.

■ ASSOCIATED CONTENT

Supporting Information

The Supporting Information is available free of charge at https://pubs.acs.org/doi/10.1021/acsami.2c00500.

Detailed experimental process and characterization methods; proton conductivity characterization; and fuel cell assembly (PDF)

https://doi.org/10.1021/acsami.2c00500
ACS Appl. Mater. Interfaces 2022, 14, 9264−9271

AUTHOR INFORMATION

Corresponding Authors

Jiang Liu − *Jiangsu Key Laboratory of Biofunctional Materials, School of Chemistry and Materials Science, Nanjing Normal University, Nanjing 210023, China*; Email: liuj@njnu.edu.cn

Lin Zeng − *Department of Mechanical and Energy Engineering, Southern University of Science and Technology, Shenzhen 518055, China; Key Laboratory of Energy Conversion and Storage Technologies (Southern University of Science and Technology), Ministry of Education, Shenzhen 518055, China*; orcid.org/0000-0002-0510-1754; Email: zengl3@sustech.edu.cn

Authors

Xiao-Min Li − *Department of Mechanical and Energy Engineering, Southern University of Science and Technology, Shenzhen 518055, China*

Yameng Wang − *Department of Mechanical and Energy Engineering, Southern University of Science and Technology, Shenzhen 518055, China*

Yongbiao Mu − *Department of Mechanical and Energy Engineering, Southern University of Science and Technology, Shenzhen 518055, China*

Ya-Qian Lan − *School of Chemistry, South China Normal University, Guangzhou 510006, China*

Complete contact information is available at: https://pubs.acs.org/10.1021/acsami.2c00500

Author Contributions

[⊥]X.-M.L. and Y.W. contributed equally to this work. The manuscript was written through contributions of all authors. All authors have given approval to the final version of the manuscript.

Notes

The authors declare no competing financial interest.

ACKNOWLEDGMENTS

This work was financially supported by the Shenzhen Fundamental Research Programs (No. JCYJ20190809143815709), the Guangdong Natural Science Foundation (No. 2021A1515010412), and the Guangdong-Hong Kong-Macao Joint Laboratory for Photonic-Thermal-Electrical Energy Materials and Devices, Southern University of Science and Technology (2019B121205001). The authors acknowledge the technical support from SUSTech Core Research Facilities.

REFERENCES

(1) Ye, Y.; Gong, L.; Xiang, S.; Zhang, Z.; Chen, B. Metal−Organic Frameworks as a Versatile Platform for Proton Conductors. *Adv. Mater.* **2020**, *32*, No. 1907090.

(2) Ellingsen, L. A.-W.; Hung, C. R.; Majeau-Bettez, G.; Singh, B.; Chen, Z.; Whittingham, M. S.; Strømman, A. H. Nanotechnology for Environmentally Sustainable Electromobility. *Nat. Nanotechnol.* **2016**, *11*, 1039−1051.

(3) Ramaswamy, P.; Wong, N. E.; Shimizu, G. K. H. MOFs as Proton Conductors − Challenges and Opportunities. *Chem. Soc. Rev.* **2014**, *43*, 5913−5932.

(4) Laberty-Robert, C.; Vallé, K.; Pereira, F.; Sanchez, C. Design and Properties of Functional Hybrid Organic−Inorganic Membranes for Fuel Cells. *Chem. Soc. Rev.* **2011**, *40*, 961−1005.

(5) Gui, D.; Duan, W.; Shu, J.; Zhai, F.; Wang, N.; Wang, X.; Xie, J.; Li, H.; Chen, L.; Diwu, J.; Chai, Z.; Wang, S. Persistent Superprotonic Conductivity in the Order of 10^{-1} S·cm^{-1} Achieved Through Thermally Induced Structural Transformation of a Uranyl Coordination Polymer. *CCS Chem.* **2019**, *1*, 197−206.

(6) Gui, D.; Dai, X.; Tao, Z.; Zheng, T.; Wang, X.; Silver, M. A.; Shu, J.; Chen, L.; Wang, Y.; Zhang, T.; Xie, J.; Zou, L.; Xia, Y.; Zhang, J.; Zhang, J.; Zhao, L.; Diwu, J.; Zhou, R.; Chai, Z.; Wang, S. Unique Proton Transportation Pathway in a Robust Inorganic Coordination Polymer Leading to Intrinsically High and Sustainable Anhydrous Proton Conductivity. *J. Am. Chem. Soc.* **2018**, *140*, 6146−6155.

(7) Paddison, S. J. Proton Conduction Mechanisms at Low Degrees of Hydration in Sulfonic Acid−Based Polymer Electrolyte Membranes. *Annu. Rev. Mater. Res.* **2003**, *33*, 289−319.

(8) Kusoglu, A.; Weber, A. Z. New Insights into Perfluorinated Sulfonic-Acid Ionomers. *Chem. Rev.* **2017**, *117*, 987−1104.

(9) Park, C. H.; Lee, S. Y.; Hwang, D. S.; Shin, D. W.; Cho, D. H.; Lee, K. H.; Kim, T.-W.; Kim, T.-W.; Lee, M.; Kim, D.-S.; Doherty, C. M.; Thornton, A. W.; Hill, A. J.; Guiver, M. D.; Lee, Y. M. Nanocrack-Regulated Self-humidifying Membranes. *Nature* **2016**, *532*, 480−483.

(10) Jana, K. K.; Srivastava, A.; Parkash, O.; Avasthi, D. K.; Rana, D.; Shahi, V. K.; Maiti, P. Nanoclay and Swift Heavy Ions Induced Piezoelectric and Conducting Nanochannel Based Polymeric Membrane for Fuel Cell. *J. Power Sources* **2016**, *301*, 338−347.

(11) Wei, M.-J.; Fu, J.-Q.; Wang, Y.-D.; Zhang, Y.; Zang, H.-Y.; Shao, K.-Z.; Li, Y.-G.; Su, Z.-M. Highly Tuneable Proton-Conducting Coordination Polymers Derived from a Sulfonate-Based Ligand. *CrystEngComm* **2017**, *19*, 7050−7056.

(12) Joarder, B.; Lin, J.-B.; Romero, Z.; Shimizu, G. K. H. Single Crystal Proton Conduction Study of a Metal Organic Framework of Modest Water Stability. *J. Am. Chem. Soc.* **2017**, *139*, 7176−7179.

(13) Sadakiyo, M.; Ōkawa, H.; Shigematsu, A.; Ohba, M.; Yamada, T.; Kitagawa, H. Promotion of Low-Humidity Proton Conduction by Controlling Hydrophilicity in Layered Metal-Organic Frameworks. *J. Am. Chem. Soc.* **2012**, *134*, 5472−5475.

(14) Amarasekara, A. S. Acidic Ionic Liquids. *Chem. Rev.* **2016**, *116*, 6133−6183.

(15) Armand, M.; Endres, F.; MacFarlane, D. R.; Ohno, H.; Scrosati, B. Ionic-Liquid Materials for the Electrochemical Challenges of the Future. *Nat. Mater.* **2009**, *8*, 621−629.

(16) Sun, X.-L.; Deng, W.-H.; Chen, H.; Han, H.-L.; Taylor, J. M.; Wan, C.-Q.; Xu, G. A Metal−Organic Framework Impregnated with a Binary Ionic Liquid for Safe Proton Conduction above 100 °C. *Chem. - Eur. J.* **2017**, *23*, 1248−1252.

(17) Fujie, K.; Otsubo, K.; Ikeda, R.; Yamada, T.; Kitagawa, H. Low Temperature Ionic Conductor: Ionic Liquid Incorporated within a Metal−Organic Framework. *Chem. Sci.* **2015**, *6*, 4306−4310.

(18) Yoshida, Y.; Fujie, K.; Lim, D.-W.; Ikeda, R.; Kitagawa, H. Superionic Conduction over a Wide Temperature Range in a Metal−Organic Framework Impregnated with Ionic Liquids. *Angew. Chem., Int. Ed.* **2019**, *58*, 10909−10913.

(19) Li, X.-M.; Wang, Y.; Wu, B.; Zeng, L. Efficient Proton Transport in Stable Functionalized Channels of Zirconium Metal−Organic Frameworks. *ACS Appl. Energy Mater.* **2021**, *4*, 8303−8310.

(20) Tuffnell, J. M.; Morzy, J. K.; Kelly, N. D.; Tan, R.; Song, Q.; Ducati, C.; Bennett, T. D.; Dutton, S. E. Comparison of the Ionic Conductivity Properties of Microporous and Mesoporous MOFs Infiltrated with a Na-ion Containing IL Mixture. *Dalton Trans.* **2020**, *49*, 15914−15924.

(21) Guo, Z.; Zheng, W.; Yan, X.; Dai, Y.; Ruan, X.; Yang, X.; Li, X.; Zhang, N.; He, G. Ionic Liquid Tuning Nanocage Size of MOFs through a Two-Step Adsorption/Infiltration Strategy for Enhanced Gas Screening of Mixed-Matrix Membranes. *J. Membr. Sci.* **2020**, *605*, No. 118101.

(22) Kinik, F. P.; Uzun, A.; Keskin, S. Ionic Liquid/Metal−Organic Framework Composites: From Synthesis to Applications. *ChemSusChem* **2017**, *10*, 2842−2863.

(23) Wang, Z.; Wang, Z.; Yang, L.; Wang, H.; Song, Y.; Han, L.; Yang, K.; Hu, J.; Chen, H.; Pan, F. Boosting Interfacial Li^+ Transport

with a MOF-Based Ionic Conductor for Solid-State Batteries. *Nano Energy* **2018**, *49*, 580−587.
(24) Wang, Z.; Tan, R.; Wang, H.; Yang, L.; Hu, J.; Chen, H.; Pan, F. A Metal−Organic-Framework-Based Electrolyte with Nanowetted Interfaces for High-Energy-Density Solid-State Lithium Battery. *Adv. Mater.* **2018**, *30*, No. 1704436.
(25) Zhao, R.; Wu, Y.; Liang, Z.; Gao, L.; Xia, W.; Zhao, Y.; Zou, R. Metal−Organic Frameworks for Solid-State Electrolytes. *Energy Environ. Sci.* **2020**, *13*, 2386−2403.
(26) Wang, S.-S.; Yang, G.-Y. Recent Advances in Polyoxometalate-Catalyzed Reactions. *Chem. Rev.* **2015**, *115*, 4893−4962.
(27) Cronin, L.; Müller, A. From Serendipity to Design of Polyoxometalates at the Nanoscale, Aesthetic Beauty and Applications. *Chem. Soc. Rev.* **2012**, *41*, 7333−7334.
(28) Li, Z.; Zhang, J.; Lin, L.-D.; Liu, J.-H.; Li, X.-X.; Zheng, S.-T. Inorganic−Organic Hybrid High-Dimensional Polyoxotantalates and Their Structural Transformations Triggered by Water. *Chem. Commun.* **2019**, *55*, 11735−11738.
(29) Peng, Q.; Li, S.; Wang, R.; Liu, S.; Xie, L.; Zhai, J.; Zhang, J.; Zhao, Q.; Chen, X. Lanthanide Derivatives of Ta/W Mixed-Addendum POMs as Proton-Conducting Materials. *Dalton Trans.* **2017**, *46*, 4157−4160.
(30) Liu, Y.; Yang, X.; Miao, J.; Tang, Q.; Liu, S.; Shi, Z.; Liu, S. Polyoxometalate-Functionalized Metal−Organic Frameworks with Improved Water Retention and Uniform Proton-Conducting Pathways in Three Orthogonal Directions. *Chem. Commun.* **2014**, *50*, 10023−10026.
(31) Xiao, H.-P.; Zhang, R.-T.; Li, Z.; Xie, Y.-F.; Wang, M.; Ye, Y.-D.; Sun, C.; Sun, Y.-Q.; Li, X.-X.; Zheng, S.-T. Organoamine-Directed Assembly of 5p−4f Heterometallic Cluster Substituted Polyoxometalates: Luminescence and Proton Conduction Properties. *Inorg. Chem.* **2021**, *60*, 13718−13726.
(32) Cao, X.-L.; Xie, S.-L.; Li, S.-L.; Dong, L.-Z.; Liu, J.; Liu, X.-X.; Wang, W.-B.; Su, Z.-M.; Guan, W.; Lan, Y.-Q. A Well-Established POM-based Single-Crystal Proton-Conducting Model Incorporating Multiple Weak Interactions. *Chem. - Eur. J.* **2018**, *24*, 2365−2369.
(33) Hupp, J. T.; Poeppelmeier, K. R. Chemistry. Better Living Through Nanopore Chemistry. *Science* **2005**, *309*, 2008−2009.
(34) Chen, C.; Wu, A.; Yan, H.; Xiao, Y.; Tian, C.; Fu, H. Trapping $[PMo_{12}O_{40}]^{3-}$ Clusters into Pre-synthesized ZIF-67 toward Mox-CoxC Particles Confined in Uniform Carbon Polyhedrons for Efficient Overall Water Splitting. *Chem. Sci.* **2018**, *9*, 4746−4755.
(35) Miao, J.; Wan, H.; Shao, Y.; Guan, G.; Xu, B. Acetalization of Carbonyl Compounds Catalyzed by Acidic Ionic Liquid Immobilized on Silica Gel. *J. Mol. Catal. A: Chem.* **2011**, *348*, 77−82.
(36) Lim, D.-W.; Kitagawa, H. Rational Strategies for Proton-Conductive Metal−Organic Frameworks. *Chem. Soc. Rev.* **2021**, *50*, 6349−6368.
(37) Lim, D.-W.; Kitagawa, H. Proton Transport in Metal−Organic Frameworks. *Chem. Rev.* **2020**, *120*, 8416−8467.
(38) Abednatanzi, S.; Leus, K.; Derakhshandeh, P. G.; Nahra, F.; De Keukeleere, K.; Van Hecke, K.; Van Driessche, I.; Abbasi, A.; Nolan, S. P.; Der Voort, P. V. POM@IL-MOFs − Inclusion of POMs in Ionic Liquid Modified MOFs to Produce Recyclable Oxidation Catalysts. *Catal. Sci. Technol.* **2017**, *7*, 1478−1487.
(39) Wan, H.; Chen, C.; Wu, Z.; Que, Y.; Feng, Y.; Wang, W.; Wang, L.; Guan, G.; Liu, X. Encapsulation of Heteropolyanion-Based Ionic Liquid within the Metal−Organic Framework MIL-100(Fe) for Biodiesel Production. *ChemCatChem* **2015**, *7*, 441−449.
(40) Li, X.-M.; Dong, L.-Z.; Li, S.-L.; Xu, G.; Liu, J.; Zhang, F.-M.; Lu, L.-S.; Lan, Y.-Q. Synergistic Conductivity Effect in a Proton Sources-Coupled Metal−Organic Framework. *ACS Energy Lett.* **2017**, *2*, 2313−2318.
(41) Li, X.-M.; Liu, J.; Zhao, C.; Zhou, J.-L.; Zhao, L.; Li, S.-L.; Lan, Y.-Q. Strategic Hierarchical Improvement of Superprotonic Conductivity in a Stable Metal−Organic Framework System. *J. Mater. Chem. A* **2019**, *7*, 25165−25171.
(42) Hurd, J. A.; Vaidhyanathan, R.; Thangadurai, V.; Ratcliffe, C. I.; Moudrakovski, I. L.; Shimizu, G. K. H. Anhydrous Proton Conduction at 150 °C in a Crystalline Metal-Organic Framework. *Nat. Chem.* **2009**, *1*, 705−710.
(43) Xue, W.-L.; Deng, W.-H.; Chen, H.; Liu, R.-H.; Taylor, J. M.; Li, Y.-k.; Wang, L.; Deng, Y.-H.; Li, W.-H.; Wen, Y.-Y.; Wang, G.-E.; Wan, C.-Q.; Xu, G. MOF-Directed Synthesis of Crystalline Ionic Liquids with Enhanced Proton Conduction. *Angew. Chem., Int. Ed.* **2021**, *60*, 1290−1297.
(44) Lee, Y. J.; Bingöl, B.; Murakhtina, T.; Sebastiani, D.; Meyer, W. H.; Wegner, G.; Spiess, H. W. High-Resolution Solid-State NMR Studies of Poly(vinyl phosphonic acid) Proton-Conducting Polymer: Molecular Structure and Proton Dynamics. *J. Phys. Chem. B* **2007**, *111*, 9711−9721.
(45) Goward, G. R.; Schuster, M. F. H.; Sebastiani, D.; Schnell, I.; Spiess, H. W. High-Resolution Solid-State NMR Studies of Imidazole-Based Proton Conductors: Structure Motifs and Chemical Exchange from ^{1}H NMR. *J. Phys. Chem. B* **2002**, *106*, 9322−9334.
(46) Brunklaus, G.; Schauff, S.; Markova, D.; Klapper, M.; Müllen, K.; Spiess, H.-W. Proton Mobilities in Phosphonic Acid-Based Proton Exchange Membranes Probed by ^{1}H and ^{2}H Solid-State NMR Spectroscopy. *J. Phys. Chem. B* **2009**, *113*, 6674−6681.
(47) Yang, Q.; Wang, Y.; Shang, Y.; Du, J.; Yin, J.; Liu, D.; Kang, Z.; Wang, R.; Sun, D.; Jiang, J. Three Hydrogen-Bonded Organic Frameworks with Water-Induced Single-Crystal-to-Single-Crystal Transformation and High Proton Conductivity. *Cryst. Growth Des.* **2020**, *20*, 3456−3465.
(48) Sadakiyo, M.; Yamada, T.; Kitagawa, H. Proton Conductivity Control by Ion Substitution in a Highly Proton-Conductive Metal−Organic Framework. *J. Am. Chem. Soc.* **2014**, *136*, 13166−13169.

https://doi.org/10.1021/acsami.2c00500
ACS Appl. Mater. Interfaces 2022, 14, 9264−9271